

Force-Regulated State Transitions of Growing Axons

Huanxin Zhang¹, Kaixuan Zhang, Min Li, Yue Shao,^{*} and Xi-Qiao Feng^{1,†}*Institute of Biomechanics and Medical Engineering, AML, Department of Engineering Mechanics, Tsinghua University, Beijing 100084, China* (Received 16 March 2022; accepted 17 August 2022; published 12 September 2022)

Growing axons are one-dimensional active structures that are important for wiring the brain and repairing nerves. However, the biophysical mechanisms underlying the complex kinetics of growing axons remain elusive. Here, we develop a theoretical framework to recapitulate force-regulated states and their transitions in growing axons. We demonstrate a unique negative feedback mechanism that defines four distinct kinetic states in a growing axon, whose transitional boundaries depend on the interplay between cytoskeletal dynamics and axon-substrate adhesion. A phase diagram for axonal growth is formulated based on two dimensionless numbers.

DOI: 10.1103/PhysRevLett.129.128101

The growth of one-dimensional structures is a universal phenomenon in physical and living systems, e.g., nanowires [1] and nerves [2,3]. During the development, remodeling, and regeneration of the brain, axons are of importance for shaping the nervous system [3–7]. Active forces generated by the cytoskeleton and extracellular environment play a key role in axonal growth [2,8–10]. However, it remains unclear how forces dictate the growth kinetics and state transitions of axons. Experiments have observed that the axonal growth is regulated by the dynamic assembly of the cytoskeleton exhibiting mechanosensitive growth kinetics [11–14]. Three states, i.e., growth, stalling, and collapse, have been observed in axons during nerve development or regeneration [15–19]. The growth state of an axon has also been shown to be determined by endogenous or exogenous forces [8,20–23]. However, the mechanism underlying the force-dependent growth kinetics and the state transitions of axons is poorly understood. In this study, we establish an active viscoelastic rod model, which integrates endogenous actomyosin contractility and exogenous axon-substrate adhesion, to describe the mechanobiochemical coupling that dictates the growth kinetics of axons. We also apply this theory to explain and predict the force-regulated state transition during the axonal growth.

Model.—We consider the motion of an axon mediated by its growth cone and actomyosin-rich distal structure [Fig. 1(a)]. The growth cone pulls the substrate through focal adhesion and active contractile forces [24–26]. Because of the constraint of the substrate, the active actomyosin contraction generates a tensile force, called the towing force, to pull the axon [27]. In contrast, the axon-substrate adhesion tends to hinder the shaft motion [28]. The axonal shaft consists of a cortex of periodic actin filaments, a core of neurofilaments, and para-axially aligned and bundled microtubules [14]. We model the shaft as an active viscoelastic rod integrating all these

cytoskeletal properties, which were only considered partially in previous models [9,23,28–30]. The shaft is subject to the towing force at the tip and the axon-substrate

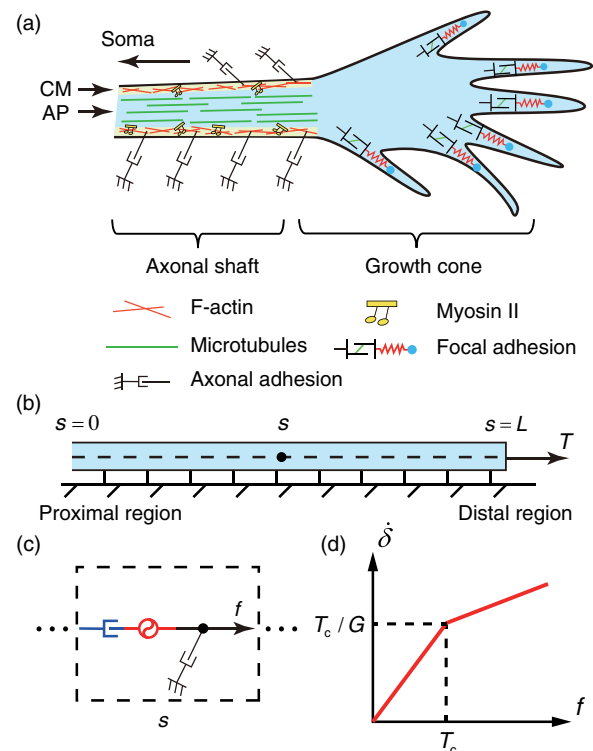


FIG. 1. (a) Schematics of an axon extending from soma depicting cytoplasmic regions and cytoskeletal structures, including axoplasm (AP) and cortical membrane (CM) of actin filaments (F-actin). (b) The rod model for a growing axon. (c) The mechanical response of the axon is depicted by a growth dashpot (blue element) connected to an actomyosin contractile element (red element) in series. The axon-substrate adhesion is simplified as a friction dashpot (black element). (d) The elongation rate $\dot{\delta}(s)$ depends on the tension $f(s)$, where T_c is the characteristic tension of actomyosin motors.

adhesion [Fig. 1(b)]. The shaft structure, its mechanical properties, and the active forces synergistically determine the growth kinetics of axons [15,22,31–33].

The growth rate of the axon is elicited by the towing force T . Let s denote the distance from the base ($s = 0$) to the tip ($s = L$), where L is the axonal length. We further incorporate a growth dashpot connected to an actomyosin contractile element in series, which share a common tension $f(s)$ [Fig. 1(c)]. The dashpot represents the growth of the microtubule-rich axoplasm. Several stress-based or strain-based laws have been proposed to model single axonal growth [8,9,22,27–29,34,35]. An exponential relation is used to describe the growth rate, i.e., $\dot{\delta}_g(s) = f(s)/G$ [9,34,35], where G is a kinetic parameter equivalent to the viscosity [28–30]. Besides, the contractile element accounts for the activity of actomyosin motors [16,34–36] and satisfies the relation [22,37] $\dot{\delta}_c(s) = c_0[1 - f(s)/T_c]$. The contractile rate $\dot{\delta}_c$ decreases with $f(s)$ in the positive load region, and has a max contractile rate c_0 at null tension. In addition, $\dot{\delta}_c$ vanishes at a characteristic tension T_c [37,38] and in the negative load region or stress-free states [39], as described by Eq. (7) in the Supplementary Material [40]. Thus, the force-regulated cytoskeleton kinetics not only drives axonal growth, but also produces contraction that limits growth, and the elongation rate $\dot{\delta}(s)$ becomes [Fig. 1(d)]

$$\dot{\delta}(s) = \begin{cases} \left(\frac{1}{G} + \frac{c_0}{T_c}\right)f(s) - c_0, & \text{for } f(s) \leq T_c, \\ \frac{f(s)}{G}, & \text{for } f(s) > T_c. \end{cases} \quad (1)$$

The axon-substrate adhesion is modeled by a dashpot with friction coefficient ζ . The frictional force is expressed as $f_r(s) = -\zeta v(s)$, where the velocity of the axon $v(s)$ is summed by the elongation rate $\dot{\delta}$ from the base to position s : $v(s) = \int_0^s \dot{\delta}(x)dx$. According to force equilibrium, the tension is described by $f(s) = T - \int_L^s f_r(y)dy$. Since the contractile rate $\dot{\delta}_c(s)$ vanishes when $f(s) > T_c$ [Eq. (1)], there are two distinct regimes of growth kinetics: low- and high-tension regimes [Fig. 2(a)], as discussed below, respectively.

Low-tension regime.—The global force in the axon is below the characteristic tension T_c , i.e., $f(s) \leq T_c$. Therefore, the tension is given by

$$f(s) = T - \zeta \int_s^L \int_0^y \left[\left(\frac{1}{G} + \frac{c_0}{T_c} \right) f(x) - c_0 \right] dx dy. \quad (2)$$

From Eq. (2), the analytic solution is derived as

$$f(s) = \frac{T - T_r}{\cosh(L/\ell)} \cosh(s/\ell) + T_r, \quad (3)$$

where $\ell = \sqrt{GT_c/(\zeta T_c + \zeta c_0 G)}$ and $T_r = T_c c_0 G / (T_c + c_0 G)$. Due to the adhesion, the towing force T dissipates

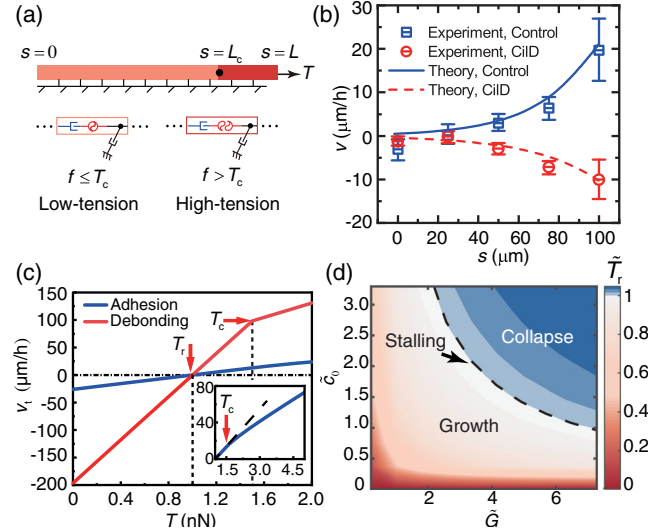


FIG. 2. Growth kinetics of the axon. (a) Schematics of two distinct tension regimes of growth kinetics. (b) Our theoretical results agree with velocities v of the normal (control) and ciliobrevin D (CilD)-treated axons of chick sensory neurons [28,41]. (c) Tip velocity v_t as a function of the towing force T in two cases: axon-substrate adhesion and debonding. Inset: details for the case of adhesion. (d) Phase diagram of the state transition defined by \tilde{c}_0 and \tilde{G} . Heat map: dimensionless rest tension \tilde{T}_r . The black dashed line represents the stalling state. Two regions are distinguished to represent collapse and growth states.

into the substrate and propagates over the characteristic length ℓ . From Eq. (2), we find $\partial f/\partial s = \zeta v(s)$, which reflects the balance of linear momentum. The velocity is determined by

$$v(s) = \frac{(T - T_r) \sinh(s/\ell)}{\zeta \ell \cosh(L/\ell)}, \quad (4)$$

and T_r is defined as the rest tension [34,36,42], at which the axon is stalling. Furthermore, the kinetic state of the entire axon can be described by the tip velocity v_t , which is obtained from Eq. (4) as

$$v_t = \frac{T - T_r}{\zeta \ell} \tanh(L/\ell). \quad (5)$$

High-tension regime.—There exists a segment of the axon near the tip where $f(s) > T_c$, wherein the motors are deactivated by the tension. Out of this segment, i.e., $s \in (0, L_c)$, the tension and velocity also follow the rules depicted by Eqs. (3) and (4) in the low-tension regime [Fig. 2(a)]. The tension in the range $s \in (L_c, L)$ is expressed as

$$f(s) = T - \zeta \int_s^L f_r^h(y) dy, \quad \text{for } s \in (L_c, L), \quad (6)$$

where the friction force in the high-tension regime denotes $f_r^h(y) = f_r^l(L_c) + \int_{L_c}^y [f(x)/G]dx$. From Eq. (6), the tension in the high-tension region is governed by

$$f(s) = \psi \{ T_c \sinh[(L-s)\sqrt{\zeta/G}] + T \sinh[(s-L_c)\sqrt{\zeta/G}] \}, \quad \text{for } s \in (L_c, L), \quad (7)$$

where the function $\psi = 1/\sinh[(L-L_c)\sqrt{\zeta/G}]$. The corresponding velocity obeys the following rule:

$$v(s) = \psi / \sqrt{\zeta G} \{ T \cosh[(s-L_c)\sqrt{\zeta/G}] - T_c \cosh[(s-L)\sqrt{\zeta/G}] \}, \quad \text{for } s \in (L_c, L). \quad (8)$$

From Eq. (8), the tip velocity is given by

$$v_t = \frac{\psi \{ T \cosh[\sqrt{\zeta/G}(L-L_c)] - T_c \}}{\sqrt{\zeta G}}. \quad (9)$$

Transitional boundary between growth, stalling, and collapse.—Previous studies employed force-calibrated needles to measure active forces and the growth kinetics of the axon [16,28,34,41,43–45]. Here, our theory successfully recapitulates force-regulated growth and retraction of chick sensory neuron axons [41], which moves forward in a finite distal region and retracts in response to dynein-mediated microtubule depletion [Fig. 2(b)]. The growth kinetics of the entire axon is described by the tip velocity in Eqs. (5) and (9). The kinetic states depend on the growth of the microtubule-rich axoplasm and actomyosin contractility, and the axon-substrate adhesion [Figs. 2(c) and 2(d)]. We also consider the special case: axon-substrate debonding ($\zeta \rightarrow 0$), as observed in previous experiments [16,17,35,46]. We find that the tip velocity and the towing force obey a piecewise linear relation [red line in Fig. 2(c)], i.e., $v_t^d = (L/G + c_0 L/T_c)T - c_0 L$ for the low-tension regime, and $v_t^d = (L/G)T$ for the high-tension regime. The results find that the transitional boundary between the growth ($v_t > 0$), stalling ($v_t = 0$), and collapse ($v_t < 0$) is $T = T_r$ [Fig. 2(c)]. Consequently, the kinetic states are governed by the dimensionless rest tension, $\tilde{T}_r = T_r/T$. Additionally, the turning point in Fig. 2(c) is determined by T_c . Due to actomyosin contractility, the slope of the tip velocity significantly decreases when $T > T_c$.

Because the rest tension T_r depends on the cytoskeletal properties, the phase diagram of kinetic states can be obtained in the $\tilde{c}_0 - \tilde{G}$ plane [Fig. 2(d)]. By taking $\tilde{T}_r = 1$, the transitional boundary of kinetic states is governed by

$$\tilde{c}_0 = \frac{q\tilde{T}_c}{\tilde{G}\tilde{T}_c - \tilde{G}}, \quad (10)$$

where \tilde{c}_0 and \tilde{G} represent the dimensionless max contractile rate and axonal kinetic parameter, respectively. We take

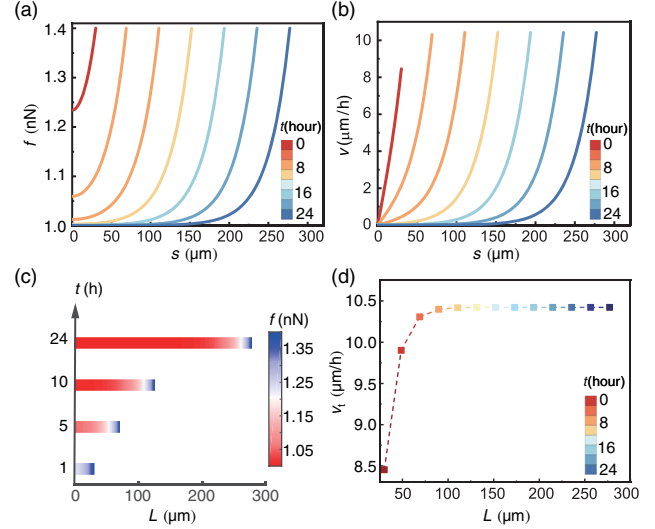


FIG. 3. Kinetic features of the growing axon. Spatiotemporal kinetics of (a) tension f and (b) velocity v under a reference towing force, 1.4 nN, during the axonal growth. (c) Stress contour at different ages. (d) Tip velocity v_t vs length L .

$\tilde{c}_0 = c_0/\bar{c}_0$ and $\tilde{G} = G/\bar{G}$, where \bar{c}_0 and \bar{G} are the reference values shown in Table S1 of the Supplemental Material [40,47], $q = T/(\bar{c}_0\bar{G})$, and $\tilde{T}_c = T_c/T$.

Kinetic features of a growing axon.—At the early age, the force generated at the growth cone is not fully dispersed along the length, and the tension profile exhibits an exponential shape [Fig. 3(a)]. Once the axon is long enough ($L \geq \ell$), in the segment beyond 1 kinetic characteristic length away from the tip, tension dissipates to the rest tension, with the velocity reducing to zero [Figs. 3(a) and 3(b)]. The stress contour shows that the mature axon has a stretching region in the distal region and a lagging region in the proximal region where the tension maintains the rest tension [Fig. 3(c)]. Furthermore, the tip velocity first increases until $L \geq \ell$ and finally reaches a maximum [Fig. 3(d)]. Applying a Gaussian function of the contractility [27,35,48,49], instead of the piecewise linear function, also results in similar kinetic features [40].

Regulatory mechanism of axon-substrate adhesion and cytoskeletal properties.—For long axons, the proximal boundary does not affect the tip velocity [Fig. 3(d)]. Therefore, we consider that the kinetic behaviors depend on cytoskeletal properties and axon-substrate adhesion. The damping of the substrate weakens the axonal growth [Fig. 4(a)]. The larger adhesion shortens the kinetic characteristic length ℓ and has no effect on the rest tension T_r [Fig. 4(d)]. For strong adhesion, the kinetic behavior is a tip grow process. However, when the axon is detached from the substrate, the velocity profile only depends on the cytoskeletal properties and reduces to linear. We further discuss the regulatory mechanism of cytoskeletal properties on the growth kinetics. Our theoretical results show that both kinetic parameter \tilde{G} and max contractile rate \tilde{c}_0

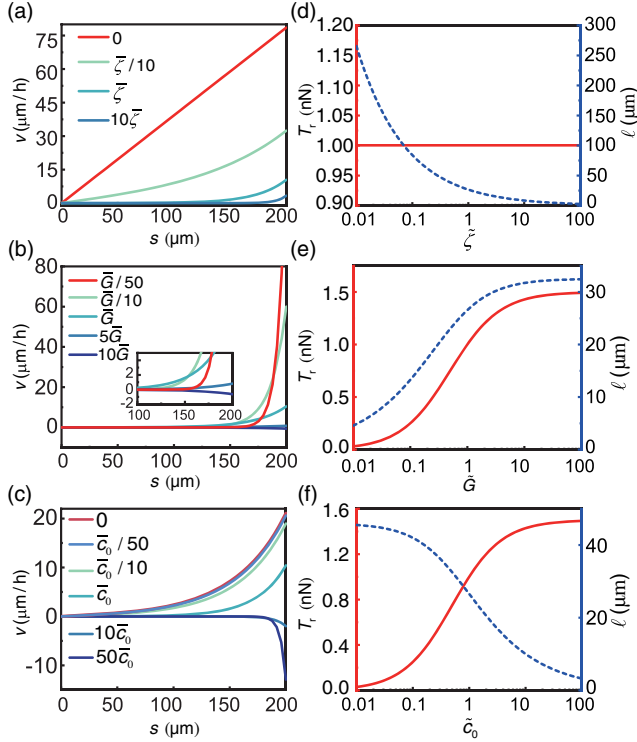


FIG. 4. Effects of axon-substrate adhesion and cytoskeletal properties on the kinetic behaviors. (a)–(c) Velocity v for different $\tilde{\zeta}$, \tilde{G} , and $\tilde{\delta}_c$, respectively. (d)–(f) Rest tension T_r and kinetic characteristic length ℓ versus $\tilde{\zeta}$, \tilde{G} , and $\tilde{\delta}_c$, respectively. Other parameters: $L = 200 \mu\text{m}$, $T = 1.4 \text{ nN}$.

impede the velocity [Figs. 4(b) and 4(c)]. The kinetic parameter describes the resistance to the growth of the microtubule-rich axoplasm, determined by the axonal physiological state. As \tilde{G} increases, the axon becomes stiffer, and forces are insufficient to drive the growth [Eq. (1)], even causing collapse [Fig. 4(b)]. This is because a higher kinetic parameter can promote the rest tension T_r and result in the state transition [Fig. 2(d)]. Additionally, a higher kinetic parameter enhances the resistance to tension, lengthening the kinetic characteristic length ℓ [Fig. 4(e)]. The max contractile rate is determined by the number of activated actomyosin motors. The increasing max contractile rate generates the stronger rest tension T_r , hindering the axonal growth [Figs. 4(c) and 4(f)]. However, enhancing the maximal contractile rate can shorten the kinetic characteristic length ℓ [Fig. 4(f)]. This is because the enhanced contractile rate $\tilde{\delta}_c$ might cause a slower forward flow.

Transition of the kinetic states.—To gain deeper insights into the force-regulated kinetics, we further investigate the velocity-tension relation. We first normalize the kinetic equations for the velocity v and tension f [40], and analyze the role of the axon-substrate adhesion and cytoskeletal properties in the dimensionless \tilde{v} - \tilde{f} relation. We find that

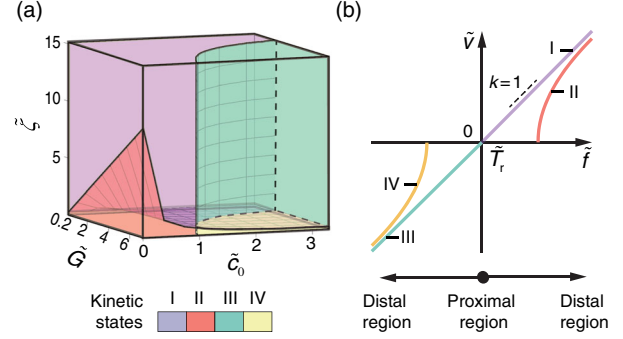


FIG. 5. Four kinetic states with transitional boundaries governed by two dimensionless numbers. (a) Phase diagram of the growth kinetics, obtained by examining the dimensionless velocity \tilde{v} and tension \tilde{f} relation. Parameter space $(\tilde{G}, \tilde{c}_0, \tilde{\zeta})$ is split by two transitional boundaries [Eqs. (10) and (11)]. (b) \tilde{v} - \tilde{f} relations of four kinetic states: (I) linear growth, (II) nonlinear growth, (III) linear collapse, and (IV) nonlinear collapse. Parameters used in the calculations are included in Table S1 of the Supplemental Material [40].

there are four distinct kinetic states governed by two transitional boundaries for the parameter space: \tilde{G} , \tilde{c}_0 , and $\tilde{\zeta}$ [Fig. 5(a)]. One of the boundaries has been given by Eq. (10), which roughly distinguishes the kinetic states: growth, stalling, or collapse. However, two different states emerge in the growth or collapse state: linear and nonlinear states [Fig. 5(b)]. The two states reflect the different dissipation rates of forces. This is because the cytoskeletal properties and axon-substrate adhesion regulate the kinetic characteristic length ℓ [Figs. 4(d)–4(f)]. With the axonal growth, the kinetic feature transits from state II to I [Figs. 3(a) and 3(b)]. Therefore, we introduce the dimensionless axonal length $\tilde{L} = L/\ell$, which reflects the characteristic length of axonal growth against axon-substrate adhesion. From the dimensionless analysis, the other transitional boundary is governed by [40]

$$\tilde{\zeta} = p\tilde{T}_r m^2, \quad (11)$$

where $\tilde{\zeta}$ represents the dimensionless friction coefficient, i.e., $\tilde{\zeta} = \zeta/\zeta_0$, where ζ_0 is the reference value shown in Table S1 of the Supplemental Material [40]. The dimensionless number $p = T/(\tilde{c}_0\tilde{\zeta}L^2)$, and m is the force propagation index. As m increases, the effect of the proximal boundary on the tension reduces. Additionally, the kinetic state exhibits a slow transition from nonlinear to linear with a slope close to 1 [Fig. 5(b)]. Therefore, the dimensionless rest tension \tilde{T}_r and axonal length \tilde{L} are two critical parameters to direct the growth kinetics. Of note, our theoretical results [Fig. 2(b)] agree with previous experimental observation (states I and III) [41], while there is still a lack of direct experimental verification of states II and IV.

Discussion.—Axonal growth is a representative model for understanding the physics of the growth kinetics of one-dimensional active structures. Our findings indicate that directional towing force is not sufficient to dictate the complex kinetics of axonal growth, largely due to the lack of additional self-regulated, negative feedbacklike mechanisms. Instead, we demonstrate that tension may provide a universal mechanism to regulate the transport and self-organization of cytoskeletal molecules and thereby define the growth kinetics and state transition of axons. This mechanism is partially analogous to the nanowire growth that is primarily dominated by the directional guidance provided by catalyst and diffusion, as well as the assembly rate of structural units [50–53]. However, for an axon, the key regulators are self-generated active forces instead of merely passive physical interactions. With our active viscoelastic rod model, we show that the force-regulated cytoskeletal properties collectively determine the state transition between growth, stalling, and collapse. In particular, the growing axon manifests four distinct kinetic states with transitional boundaries defined by the dimensionless rest tension and axonal length. They reflect the competition between actomyosin machinery of the axon shaft and the growth cone, and the characteristic length of axonal growth against axon-substrate adhesion, respectively. Our theory has expanded the knowledge beyond what was attainable with previous models [9,23,28–30]. It also provides a framework to understand how other environmental cues, such as matrix stiffness and geometry, might regulate axonal growth.

In all, this Letter established an active viscoelastic rod model of axonal growth, and applied it to elucidate kinetics and state transition. Our results demonstrated the previously unappreciated physics of the axonal growth, and provided a quantitative phase diagram to guide potential engineering of the axonal growth via modulating two key dimensionless numbers (e.g., it influences the rest tension by motor-targeting optogenetics or drugs [12,41,44] and modulates the kinetic characteristic length by modifying the substrate-cell adhesion [54]). Our model might also help predict force-regulated growth kinetics and state transition of one-dimensional active structures in other biological contexts. Our findings not only broaden the basic understanding of the physics of life, but also might help guide novel strategies for nerve regeneration in the future.

This work was supported by the National Natural Science Foundation of China (Grants No. U1932132, No. 12032014, No. 11921002, No. 11620101001, and No. 12102218), National Key R&D Program of China (2017YFF0106303), and Natural Science Foundation of Chongqing (Grant No. cstc2018jcyjAX0405). K. Z. acknowledges China Postdoctoral Science Foundation (2020M680525).

*yshao@tsinghua.edu.cn

†fengxq@tsinghua.edu.cn

- [1] V. Schmidt, J. V. Wittemann, and U. Gösele, Growth, thermodynamics, and electrical properties of silicon nanowires, *Chem. Rev.* **110**, 361 (2010).
- [2] K. Franze, Integrating chemistry and mechanics: The forces driving axon growth, *Annu. Rev. Cell Dev. Biol.* **36**, 61 (2020).
- [3] S. P. Mutalik and A. Ghose, Axonal cytomechanics in neuronal development, *J. Biosci.* **45**, 64 (2020).
- [4] O. Blanquie and F. Bradke, Cytoskeleton dynamics in axon regeneration, *Curr. Opin. Neurobiol.* **51**, 60 (2018).
- [5] S. Budday, P. Steinmann, and E. Kuhl, Physical biology of human brain development, *Front. Cell. Neurosci.* **9**, 257 (2015).
- [6] A. Chédotal and L. J. Richards, Wiring the brain: The biology of neuronal guidance, *Cold Spring Harbor Perspect. Biol.* **2**, a001917 (2010).
- [7] M. A. Holland, K. E. Miller, and E. Kuhl, Emerging brain morphologies from axonal elongation, *Ann. Biomed. Eng.* **43**, 1640 (2015).
- [8] A. Goriely, S. Budday, and E. Kuhl, *Neuromechanics: From Neurons to Brain* (Academic Press Inc., New York, 2015), Vol. 48, pp. 79–139, 10.1016/bs.aams.2015.10.002.
- [9] H. Oliveri, K. Franze, and A. Goriely, Theory for Durotactic Axon Guidance, *Phys. Rev. Lett.* **126**, 118101 (2021).
- [10] D. M. Suter and K. E. Miller, The emerging role of forces in axonal elongation, *Prog. Neurobiol.* **94**, 91 (2011).
- [11] S. C. Sousa and M. M. Sousa, The cytoskeleton as a modulator of tension driven axon elongation, *Dev. Neurobiol.* **81**, 300 (2021).
- [12] K. McElmurry, J. E. Stone, D. Ma, P. Lamoureux, Y. Zhang, M. Steidemann, L. Fix, F. Huang, K. E. Miller, and D. M. Suter, Dynein-mediated microtubule translocation powering neurite outgrowth in chick and Aplysia neurons requires microtubule assembly, *J. Cell Sci.* **133**, jcs232983 (2020).
- [13] X. F. Zhang, V. Ajeti, N. Tsai, A. Fereydooni, W. Burns, M. Murrell, E. M. D. L. Cruz, and P. Forscher, Regulation of axon growth by myosin II-dependent mechanocatalysis of cofilin activity, *J. Cell Biol.* **218**, 2329 (2019).
- [14] K. Xu, G. Zhong, and X. Zhuang, Actin, spectrin, and associated proteins form a periodic cytoskeletal structure in axons, *Science* **339**, 452 (2013).
- [15] P. Recho, A. Jérusalem, and A. Goriely, Growth, collapse, and stalling in a mechanical model for neurite motility, *Phys. Rev. E* **93**, 032410 (2016).
- [16] M. O’Toole, P. Lamoureux, and K. E. Miller, Measurement of subcellular force generation in neurons, *Biophys. J.* **108**, 1027 (2015).
- [17] T. D. Nguyen, I. B. Hogue, K. Cung, P. K. Purohit, and M. C. McAlpine, Tension-induced neurite growth in microfluidic channels, *Lab Chip* **13**, 3735 (2013).
- [18] J. Ruschel, F. Hellal, K. C. Flynn, S. Dupraz, D. A. Elliott, A. Tedeschi, M. Bates, C. Sliwinski, G. Brook, K. Dobrindt, M. Peitz, O. Brüstle, M. D. Norenberg, A. Blesch, N. Weidner, M. B. Bunge, J. L. Bixby, and F. Bradke, Systemic administration of epothilone B promotes axon regeneration after spinal cord injury, *Science* **348**, 347 (2015).
- [19] E.-M. Hur, I. H. Yang, D.-H. Kim, J. Byun, Sajilafu, W.-L. Xu, P. R. Nicovich, R. Cheong, A. Levchenko, N. Thakor,

- and F.-Q. Zhou, Engineering neuronal growth cones to promote axon regeneration over inhibitory molecules, *Proc. Natl. Acad. Sci. U.S.A.* **108**, 5057 (2011).
- [20] S. D. Vincentiis, A. Falconieri, M. Mainardi, V. Cappello, V. Scribano, R. Bizzarri, B. Storti, L. Dente, M. Costa, and V. Raffa, Extremely low forces induce extreme axon growth, *J. Neurosci.* **40**, 4997 (2020).
- [21] V. Raffa, F. Falcone, S. D. Vincentiis, A. Falconieri, M. P. Calatayud, G. F. Goya, and A. Cuschieri, Piconewton mechanical forces promote neurite growth, *Biophys. J.* **115**, 2026 (2018).
- [22] J. A. García-Grajales, A. Jérusalem, and A. Goriely, Continuum mechanical modeling of axonal growth, *Comput. Methods Appl. Mech. Eng.* **314**, 147 (2017).
- [23] H. Oliveri and A. Goriely, Mathematical models of neuronal growth, *Biomech. Model. Mechanobiol.* **21**, 89 (2022).
- [24] K. Franze and J. Guck, The biophysics of neuronal growth, *Rep. Prog. Phys.* **73**, 094601 (2010).
- [25] P. C. Kerstein, R. H. Nichol, and T. M. Gomez, Mechanochemical regulation of growth cone motility, *Front. Cell. Neurosci.* **9**, 244 (2015).
- [26] D. E. Koser, A. J. Thompson, S. K. Foster, A. Dwivedy, E. K. Pillai, G. K. Sheridan, H. Svoboda, M. Viana, L. da F. Costa, J. Guck, C. E. Holt, and K. Franze, Mechanosensing is critical for axon growth in the developing brain, *Nat. Neurosci.* **19**, 1592 (2016).
- [27] R. Bernal, P. A. Pullarkat, and F. Melo, Mechanical Properties of Axons, *Phys. Rev. Lett.* **99**, 018301 (2007).
- [28] M. O'Toole, P. Lamoureux, and K. E. Miller, A physical model of axonal elongation: Force, viscosity, and adhesions govern the mode of outgrowth, *Biophys. J.* **94**, 2610 (2008).
- [29] T. J. Dennerll, P. Lamoureux, R. E. Buxbaum, and S. R. Heidemann, The cyto mechanics of axonal elongation and retraction, *J. Cell Biol.* **109**, 3073 (1989).
- [30] T. J. Dennerll, H. C. Joshi, V. L. Steel, R. E. Buxbaum, and S. R. Heidemann, Tension and compression in the cytoskeleton of PC-12 neurites. II: Quantitative measurements, *J. Cell Biol.* **107**, 665 (1988).
- [31] K. E. Miller and D. M. Suter, An integrated cytoskeletal model of neurite outgrowth, *Front. Cell. Neurosci.* **12**, 447 (2018).
- [32] R. de Rooij, E. Kuhl, and K. E. Miller, Modeling the axon as an active partner with the growth cone in axonal elongation, *Biophys. J.* **115**, 1783 (2018).
- [33] R. de Rooij, K. E. Miller, and E. Kuhl, Modeling molecular mechanisms in the axon, *Comput. Mech.* **59**, 523 (2017).
- [34] S. Siechen, S. Y. Yang, A. Chiba, and T. Saif, Mechanical tension contributes to clustering of neurotransmitter vesicles at presynaptic terminals, *Proc. Natl. Acad. Sci. U.S.A.* **106**, 12611 (2009).
- [35] R. Bernal, F. Melo, and P. A. Pullarkat, Drag force as a tool to test the active mechanical response of PC12 neurites, *Biophys. J.* **98**, 515 (2010).
- [36] J. Rajagopalan, A. Tofangchi, and M. T. A. Saif, Drosophila neurons actively regulate axonal tension *in vivo*, *Biophys. J.* **99**, 3208 (2010).
- [37] M. J. Greenberg and J. R. Moore, The molecular basis of frictional loads in the *in vitro* motility assay with applications to the study of the loaded mechanochemistry of molecular motors, *Cytoskeleton* **67**, 273 (2010).
- [38] K. Oiwa, S. Chaen, E. Kamitsubo, T. Shimmen, and H. Sugi, Steady-state force-velocity relation in the ATP-dependent sliding movement of myosin-coated beads on actin cables *in vitro* studied with a centrifuge microscope, *Proc. Natl. Acad. Sci. U.S.A.* **87**, 7893 (1990).
- [39] F. Jülicher, K. Kruse, J. Prost, and J.-F. Joanny, Active behavior of the cytoskeleton, *Phys. Rep.* **449**, 3 (2007).
- [40] See Supplemental Material at <http://link.aps.org/supplemental/10.1103/PhysRevLett.129.128101> for details regarding theoretical derivations and parameter values, which includes Ref. [47].
- [41] D. H. Roossien, P. Lamoureux, and K. E. Miller, Cytoplasmic dynein pushes the cytoskeletal meshwork forward during axonal elongation, *J. Cell Sci.* **127**, 3593 (2014).
- [42] A. Tofangchi, A. Fan, and M. T. A. Saif, Mechanism of axonal contractility in embryonic drosophila motor neurons *in vivo*, *Biophys. J.* **111**, 1519 (2016).
- [43] T. Betz, D. Koch, Y. B. Lu, K. Franze, and J. A. Kas, Growth cones as soft and weak force generators, *Proc. Natl. Acad. Sci. U.S.A.* **108**, 13420 (2011).
- [44] P. Lamoureux, S. R. Heidemann, N. R. Martzke, and K. E. Miller, Growth and elongation within and along the axon, *Dev. Neurobiol.* **70**, 135 (2010).
- [45] A. I. M. Athamneh and D. M. Suter, Quantifying mechanical force in axonal growth and guidance, *Front. Cell. Neurosci.* **9**, 359 (2015).
- [46] J. Zheng, P. Lamoureux, V. Santiago, T. Dennerll, R. E. Buxbaum, and S. R. Heidemann, Tensile regulation of axonal elongation and initiation, *J. Neurosci.* **11**, 1117 (1991).
- [47] D. E. Moulton, T. Lessinnes, and A. Goriely, Morphoelastic rods. Part I: A single growing elastic rod, *J. Mech. Phys. Solids* **61**, 398 (2013).
- [48] R. Bernal, M. V. Hemelryck, B. Gurchenkov, and D. Cuvelier, Actin stress fibers response and adaptation under stretch, *Int. J. Mol. Sci.* **23**, 5095 (2022).
- [49] N. Gupta, A. Chaudhuri, and D. Chaudhuri, Morphological and dynamical properties of semiflexible filaments driven by molecular motors, *Phys. Rev. E* **99**, 042405 (2019).
- [50] Y.-C. Chou, K. Hillerich, J. Tersoff, M. C. Reuter, K. A. Dick, and F. M. Ross, Atomic-scale variability and control of III-V nanowire growth kinetics, *Science* **343**, 281 (2014).
- [51] C. W. Pinion, D. P. Nenon, J. D. Christesen, and J. F. Cahoon, Identifying crystallization- and incorporation-limited regimes during vapor-liquid-solid growth of si nanowires, *ACS Nano* **8**, 6081 (2014).
- [52] C. Y. Wen, J. Tersoff, M. C. Reuter, E. A. Stach, and F. M. Ross, Step-Flow Kinetics in Nanowire Growth, *Phys. Rev. Lett.* **105**, 195502 (2010).
- [53] A. Rothman, V. G. Dubrovskii, and E. Joselevich, Kinetics and mechanism of planar nanowire growth, *Proc. Natl. Acad. Sci. U.S.A.* **117**, 152 (2020).
- [54] J. Xia, Z. Y. Liu, Z. Y. Han, Y. Yuan, Y. Shao, X. Q. Feng, and D. A. Weitz, Regulation of cell attachment, spreading, and migration by hydrogel substrates with independently tunable mesh size, *Acta Biomater.* **141**, 178 (2022).